Inorganica Chimica Acta 482 (2018) 738–748

Contents lists available at ScienceDirect

Inorganica Chimica Acta

journal homepage: www.elsevier.com/locate/ica

Research paper

Synthesis, characterization, solution equilibria, DFT study, DNA binding affinity and cytotoxic properties of a cobalt(II) complex with a 5-pyrazolone ligand

Selma Akcha[a,*], Santiago Gómez-Ruiz[b,*], Safia Kellou-Tairi[c], Luis Lezama[d], Frank Blanco Pérez[e], Ouassini Benali-Baitich[a]

[a] Laboratoire d'Hydrométallurgie et Chimie Inorganique Moléculaire, Faculté de chimie, USTHB, BP 32, 16025 El-Alia, Bab Ezzouar, Alger, Algeria
[b] Departamento de Biología y Geología, Física y Química Inorgánica, Universidad Rey Juan Carlos, Móstoles, Madrid E-28933, Spain
[c] Laboratoire de Physico-chimie Théorique et de Chimie Informatique, Faculté de chimie, USTHB BP 32, El Alia, Bab Ezzouar, Alger, Algeria
[d] Departamento de Química Inorgánica y BCMaterials, Universidad del País Vasco, UPV/EHU, P.O. Box 644, E-48080 Bilbao, Spain
[e] Laboratorio de Patología Celular y Molecular, Centro de Medicina Experimental, Instituto Venezolano de Investigaciones Científicas, Apartado 20632, Caracas 1020-A, Venezuela

ARTICLE INFO

Keywords:
Cobalt
Pyrazolone
DNA-interactions
Cytotoxicity
Colon cancer
Prostate cancer

ABSTRACT

Our work describes the synthesis, the complexation and the characterization of a cobalt(II) complex with a 5-pyrazolone ligand carrying a thioamide group on N^1 position. The study of the complexation in solution allowed the determination of the stability constants of the complex and the distribution of the species involving Co(II) over the whole pH-range. The solid cobalt(II) complex has then been synthesized and fully characterized by infrared, electronic, EPR and mass spectrometries, in addition to magnetic and voltammetric measurements. The data clearly indicated an octahedral high spin Co(II) complex with two mononegative molecules of the N,S-ligand, and two water molecules, likely in a *cis* position because of the high anisotropy. DFT calculations performed on both the ligand and the complex structures allowed us to study the spectral features, and to propose the most fitting structures to the experimental data. The interaction of the 5-pyrazolone ligand and its Cobalt(II) complex with fish-sperm DNA has been studied by electronic spectrometry and cyclovoltammetry. Intercalation has been identified as a binding mode and the strength of the binding assessed. In order to explore eventual cytotoxic and/or cytostatic properties of our compounds, the ligand and the cobalt complex have been tested on PC-3 (human prostate carcinoma) and HT-29 (human colon carcinoma) using sulphorhodamine B (SRB) assay.

1. Introduction

Metal complexes are potential anticancer, antibacterial and anti-inflammatory sources [1–6]. Many coordination compounds have exhibited interesting pharmaceutical properties that can be keys in fighting virus such as HIV [7], and that act as potential candidates to cure important health issues such as the Alzheimer disease [8]. Cobalt is an essential micronutrient that exists in plants, human and animals' metabolisms. In humans, cobalt is known for its presence in the center of vitamin B12 that is necessary for many physiological processes like the synthesis of DNA and for the proper work of the nervous system [9–11]. Cobalt complexes have also aroused interest due to their pharmaceutical properties as anticancer and antimicrobial [12–14]. The success of metal complexes is closely linked with the proper choice of ligands, as they play a crucial role in the properties of the final complex [15]. Recent research has been directed towards the synthesis and the evaluation of complexes with biologically interesting ligands with the aim of widening the spectrum of the complex activity [15]. In this context pyrazolones are an important class of heterocyclic molecules that have been reported for being antimicrobial, anti-inflammatory and antitumoral agents, in addition to some pyrazolone effective against brain and myocardial ischemia [16–18]. Thus, we studied the complexation in solution of cobalt(II) with a pyrazolone ligand, we determined the complex stability constants, and the species distribution over the whole pH-range. We then carried out the synthesis and a complete characterization of the cobalt(II) complex, and performed DFT calculations in order to gain a better insight into the molecular structure of the Co(II) complex and its spectral features. We studied by UV spectrometry and cyclovoltammetry its DNA-binding affinity, and finally performed a study of its cytotoxic and cytostatic

* Corresponding authors.
E-mail addresses: sakcha@usthb.dz (S. Akcha), santiago.gomez@urjc.es (S. Gómez-Ruiz).

https://doi.org/10.1016/j.ica.2018.06.051
Received 7 February 2018; Received in revised form 24 June 2018; Accepted 28 June 2018
Available online 07 July 2018

properties toward two tumoral cell lines: PC-3 (human prostate carcinoma) and HT-29 (human colon carcinoma).

2. Experimental

2.1. Materials

All reagents used were of analytical grade, purchased from Fluka, and used without further purification. A stock solution of fish-sperm DNA (FS-DNA, Sigma-Aldrich) was prepared by dissolving the sodium salt in buffer containing 15 mM of trisodium citrate and 150 mM of NaCl at pH 7.2. The solution was stirred three days and kept at 4–5 °C for no longer than one week [19–22]. The absorbance ratio of (FS-DNA) solution at λ_{max} 260 and 280 nm (A_{260}/A_{280}) was 2:1, which showed that it was sufficiently free from protein contamination. The solution was standardized spectrophotometrically using its known molar absorbance coefficient at $\lambda = 260$ nm ($\varepsilon = 6600\ cm^{-1}\ M^{-1}$) [19–22]. No precipitation or turbidity was observed even after one week of storage. Also no changes in the electronic spectrum of this solution of DNA have been recorded. However, DNA solutions were freshly used, never exceeding 5 days of storage. Concentrated stock solutions of the ligand and the metal complex were prepared by dissolving the required quantities in dimethyl sulfoxide (DMSO). The desired concentrations were achieved by dilutions in buffer (15 mM of trisodium citrate and 150 mM of NaCl at pH 7.2). Homogeneous solutions were obtained with DMSO content less than 1%.

2.2. Physical measurements

The infrared spectra were recorded using KBr pellets on a Perkin Elmer Spectrum Two spectrophotometer. Electronic spectra were recorded in ethanol on a Jasco 350 spectrometer using quartz cells. ^1H NMR and ^{13}C NMR spectra were recorded on a 400 MHz and 100 MHz Varian Mercury FT-400 spectrometer. Mass spectra were recorded with a Brucker Daltonics DataAnalysis 3.3 using electrospray ionisation. Magnetic susceptibility measurements were carried out with applied magnetic field of 0.1 T on polycrystalline sample of the cobalt complex with a Quantum Design MPMS-XL-5 SQUID magnetometer. X-band EPR measurements were carried out on a Bruker ELEXSYS 500 spectrometer with a maximum available microwave power of 200 mW and equipped with a super-high-Q resonator ER-4123-SHQ and standard Oxford Instruments low temperature devices. The magnetic field was calibrated by an NMR probe and the frequency inside the cavity was determined with a Hewlett-Packard 5352B microwave frequency counter. Computer simulation: WINEPR-Simfonia, version 1.5, Bruker Analytische Messtechnik GmbH). Experiments of cyclic voltammetry were conducted using a potentiostat/galvanostat Autolab PGSTAT302 Metrohm.

2.3. Synthesis

2.3.1. Synthesis of the ligand H_2L

The pyrazolone derivative N-ethyl-4-(2-hydroxyethyl)-3-methyl-5-oxo-2,5-dihydro-1H-pyrazole-1-carbothioamide (H_2L) was prepared by heating 8 h under reflux, equimolar amounts of 3-acetyloxolan-2-one and *N*-ethylhydrazinecarbothioamide with 1% of Keggin catalyst ($H_4SiW_{12}O_{14}$, nH_2O) in ethanol. The white ligand was collected by filtration. Yield: 80% [19,23].

FT-IR bands: ῡ (O—H) 3496; ῡ (N—H) 3280 ; ῡ (C═O) 1639; ῡ (N—C═S) 1574 ; ῡ (C═C) 1548; ῡ (C═S) 789 [24]. ^1H NMR (DMSO-d_6, ppm): 1.18 (t, $J = 7$ Hz, 3H, $CH_{3thioamide}$), 2.16 (s, 3H, CH_3—C═C), 2.34 (q, $J = 7$ Hz, 2H, CH_2), 2.49 (m, 3H, CH_2—OH), 3.37 (t, 2H, CH_2—(CH_2OH)), 10.3 (broad, NH_{Cyclic}), 11.45 (s, NH $_{thioamide}$). ^{13}C NMR (DMSO-d_6, ppm): 17 ($CH_{3pyrazolone}$), 25.44 (CH_3 $_{thioamide}$), 59.54 (CH_2—(CH_2—OH)), 61.02 ($CH_{2thioamide}$), 136.92 (C═(C—CH_3)), 149.95 (NH—C═C), 159.65 (C═O), 174.26 (C═S). [M + Na^+], *m/z*: 252.08. UV/Visible: (λ_{max} (nm), ε ($L\ mole^{-1}\ cm^{-1}$)): 300 (12000), 277 (24000), 239 (30300).

2.3.2. Synthesis of the complex

Cobalt complex was synthesized by adding an ethanolic solution containing 0.4 mmol of the pyrazolone to 0.2 mmol of $CoCl_2{\cdot}6H_2O$ dissolved in the same solvent. The mixture which turned immediately deep green, was heated and refluxed 3 h resulting in a yield of 75%.

2.4. Potentiometric study

pH-metric readings were measured to 0.01 unit with a Schott Titroline Easy Model, standardized before titrations with buffer solutions produced by Fluka. All the solutions were introduced into a thermostated double-walled electrochemical cell that maintained a constant temperature (25 ± 0.1 °C). The measurements were conducted under nitrogen in order to avoid interference with CO_2 or O_2 gases. The following solutions were prepared in (90:10 v/v) water/ethanol and 0.2 M ionic strength (NaCl), and titrated against carbonate free NaOH 0.1 M as follows: *(i)* The solvent: 20 mL of NaCl (0.5 M) + 5 mL of absolute ethanol, completed to 50 mL in a volumetric flask with distilled water. *(ii)* Ligand solution: 20 mL of NaCl (0.5 M) + 5 mL of the ligand ($5\cdot10^{-3}$ M) + 5 mL of HCl (0.1 M), completed to 50 mL with distilled water. *(iii)* Metal-Ligand solution: 20 mL of NaCl (0.5 M) + 5 mL of the ligand ($5\cdot10^{-3}$ M) + 5 mL of $CoCl_2\cdot6H_2O$ (2.5×10^{-3} M) + 5 mL of HCl (0.1 M) completed to 50 mL with distilled water.

In order to perform a rigorous study; the metallic solution of cobalt has been titrated against ethylenediaminetetraacetic acid (EDTA) in presence of murexide to obtain its exact concentration.

The potentiometric experimental results have then been exploitable by a computational program [25], which calculated from the titration of the ligand alone its acidity constants, and in presence of Co^{2+}, the complex stability constants.

2.5. Computational methods

Quantum chemical calculations for the Pyrazolone and its Co(II) complex were performed to optimize the geometry and to obtain the spectral features using Jaguar program with the aid of Maestro GUI Schrödinger [26].

3D molecular modeling of the ligand and the complex was performed using density functional theory (DFT) at the B3LYP level for the ligand and UB3LYP for the Co(II) complex. We used Lacvp** [27] basis set which is recommended when working with transition metals. The frequency calculations of the optimized geometries were done to confirm that the optimized structures achieved the minimum energy, and to obtain the theoretical vibrational spectra by assuming C_1 point group symmetry. All frequency calculations gave positive values. Vertical electronic excitations based on optimized geometries were computed using the time-dependent density functional theory (TDDFT) formalism in ethanol, using the Poisson Boltzmann finite element method (PBF).

2.6. Electrochemistry

In order to explore the redox properties of the cobalt complex, voltametric experiments were conducted from +3.0 to −3.0 V, at room temperature with analyte concentrations of 1 mM in DMSO using 0.1 M tetrabutylammonium hexafluorophosphate as the supporting electrolyte. All solutions were purged at least 15 min with N_2. The three-electrode system consisted of a glassy carbon-working electrode, a platinum auxiliary, and a Pt reference electrode. The ferrocenium/ferrocene couple, which was added at the end of each experiment, was used to monitor the reference electrode and was observed at 0.48 V with $\Delta Ep = 0.140$ V under these conditions. All potentials are given against ferrocene.

2.7. DNA-binding experiments

2.7.1. UV–visible experiments

Transition metal complexes can bind to DNA via both covalent and/or non-covalent interactions. In the case of covalent interaction, the labile ligand of the complex can be replaced by the nitrogen or the oxygen of DNA bases such as guanine N7 or O6. This process is irreversible and may lead to metabolization issues [11,21].

The non-covalent interactions include intercalative, electrostatic, and groove (surface) binding of metal complexes outside of the DNA helix [11]. The changes observed in the UV spectrum upon titration give evidence of the existing interaction mode [20]. Hypochromism due to $\pi \rightarrow \pi$ stacking interactions appears in the case of an intercalative binding mode, hyperchromism in the case of an electrostatic binding, and a red shift (bathochromism) is usually observed when the DNA duplex is stabilized [20].

The UV spectra of the ligand and the cobalt complex have been recorded in buffer (15 mM of trisodium citrate and 150 mM of NaCl at pH 7.2) in the presence of 1% DMSO. The stability of the cobalt complex under these experimental conditions has been checked and its electronic spectrum recorded three times at different moments of storage. No changes appeared when comparing the spectra. The same bands were observed at the same positions.

UV titrations have been conducted for a constant concentration of each compound (20 μM) in the presence of increasing amounts of DNA in buffer (concentrations varying from 2 to 30–40 μM). Measurements have been conducted after addition of equal amounts of FS-DNA in both the sample solution and the reference one in order to avoid the absorbance of FS-DNA itself [19].

2.7.2. Cyclic voltammetry experiments

The interaction of the cobalt complex with DNA by cyclic voltammetry was conducted at room temperature using the buffer solution (15 mM of trisodium citrate and 150 mM of NaCl) as solvent with the supporting electrolyte. The saturated Ag/AgCl/KCl was used as the reference electrode, and 10^{-3} M analyte solutions were prepared in the mixture (buffer/DMSO) (90%/10%) [19].

2.8. Growth inhibition and cytotoxicity

The sulphorhodamine B (SRB) assay was used to evaluate the effect of the ligand H_2L and the cobalt(II) complex on the growth and viability of the two human tumor cell lines, PC-3 (human prostate carcinoma) and HT-29 (human colon carcinoma). Cells were cultured in Dulbecco's Modified Eagle's Medium (DMEM) supplemented with 10% heat-inactivated fetal bovine, (Gibco, BRL, USA) and penicillin (100 Units/mL)/streptomycin (100 μg/mL), containing in addition, 0.45% of glucose for the HT-29 cells [28,29]. Each drug was assayed in triplicate at 7 different concentrations up to a maximum of 30 μM. The concentrations inducing 50% growth inhibition (GI_{50}), total growth inhibition (TGI) and 50% cytotoxicity (LC_{50}) after a 48 h incubation period were calculated by linear interpolation from the observed data points [28,29].

3. Results and discussion

3.1. Potentiometric study

The pH-metric data obtained from the titration of the ligand H_2L at 25 ± 0.1 °C in (90:10v/v) water/ethanol and 0.2 M ionic strength, has been processed by the computational program, which allowed the calculation of its acidity constants [19,30,31]. The values of the stepwise dissociation constants pK_i corresponding to equilibria (1) and (2) are respectively $pK_1 = 6.65$ and $pK_2 = 9.90$.

Table 1
Overall and stepwise stability constants.

Complex	log β_i	log K_i
$[Co(HL)]^+$	17.65 ± 0.01	17.65
$[Co(HL)_2]$	30.47 ± 0.01	12.82

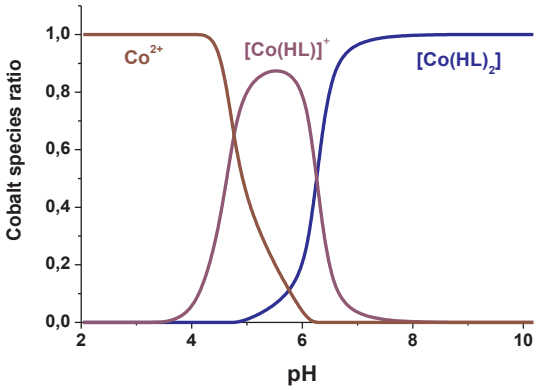

Fig. 1. Distribution curve of the cobalt species.

$$H_2L \rightleftharpoons H^+ + HL^- \quad (1)$$

$$HL^- \rightleftharpoons H^+ + L^{2-} \quad (2)$$

The program also allowed the determination of the stepwise and overall stability constants of the cobalt complex in the same conditions, and the distribution curve of the metallic species [19,30,31].

Table 1 regroups the stability constants of the complex, and Fig. 1 represents the distribution curve of the cobalt species *versus* pH.

The examination of the cobalt species distribution curve (Fig. 1) shows that in the most acidic medium, the predominant specie is the free cation. In that point, the complexation hasn't started yet. From pH 4 to pH 6, the predominant specie is the first complex $[Co(HL)]^+$ where the metal is coordinated to a single deprotonated molecule of the ligand. From pH 7, the last specie which consists of the complex $[Co(HL)_2]$ (the specie obtained in the solid state) starts forming. It is formed by the cationic cobalt linked to two equivalent deprotonated ligands.

A study of the data gathered in Table 1 shows that this cobalt complex exhibits relatively high stability constants. A comparison between these values and the ones previously reported for copper(II) and nickel(II) with the same ligand, shows that they lie within the same range [19]. Copper having as expected by Irving and Williams series, the higher stability constants. However, the cobalt complex shows in our series higher stability constants than nickel. The high stability that exhibit the complexes containing this pyarazolone-carbothioamide ligand (H_2L) is surely related to the bidentate nature of the ligand [32]. The study of the complexes' structures by several experimental techniques (like presented below) shows that this substituted pyrazolone acts as a N,S bidentate ligand that can form chelate rings. The presence of chelate rings within a complex structure confers an extra degree of stability, with stability increasing as the number of chelate rings increases [32]. The cobalt complex, as will be shown further, contains two five-membered rings, which are often considered to be the most stable [33]. The complexes with larger chelate rings would be of lower stability than those of five-membered chelate rings because of the larger volume to which the chelate ring would be restricted [33]. This chelate effect is believed to be responsible for the stability of the cobalt complex.

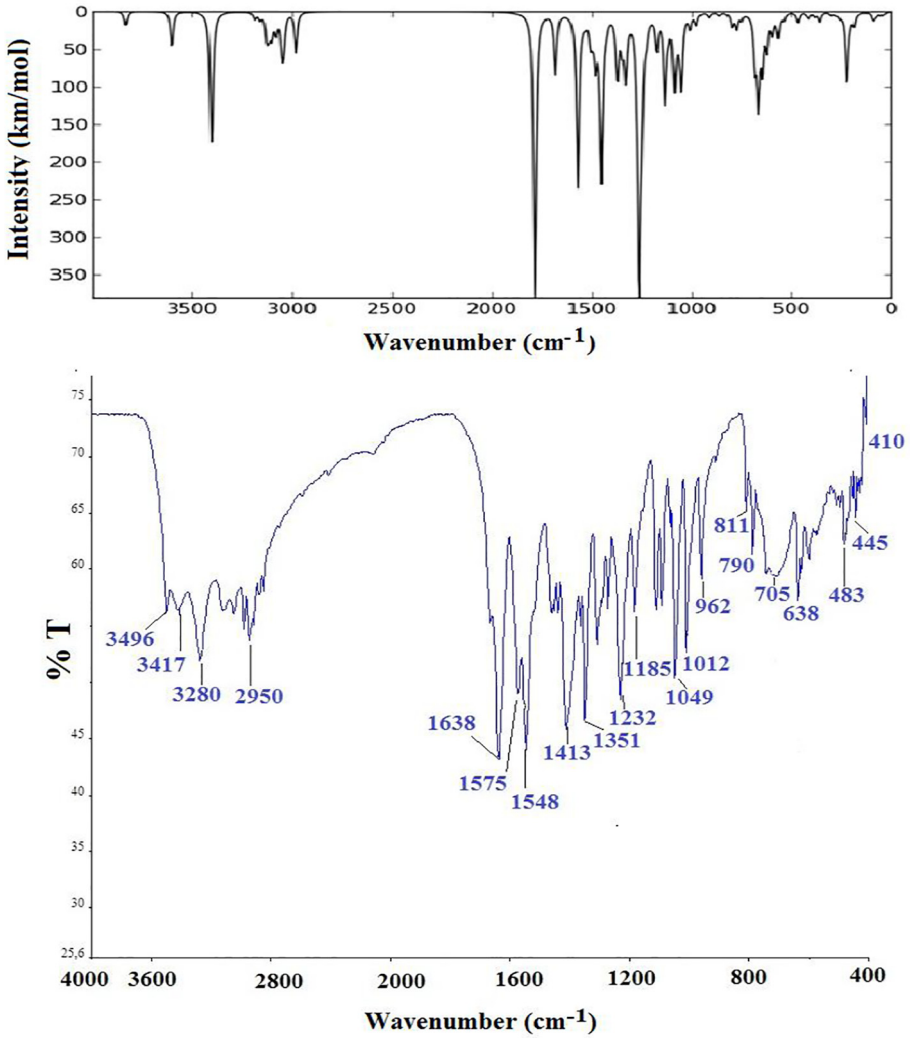

Fig. 2. Theoretical (upside) and experimental vibration spectra of the ligand H_2L.

3.2. Infrared study

A study of the complex IR spectrum and a comparison with the ligand's one reveal the following features: A broad band appears between 3200 and 3400 cm^{-1} which indicates the coordination of water molecules. The stretching band $\bar{\upsilon}$ (N—C═S) is affected by complexation and shifted toward lower frequencies by 10 cm^{-1}, which suggests its implication in coordination. A rigorous study of the cobalt spectrum shows two new bands: $\bar{\upsilon}$ (Co—O) at 501 cm^{-1} and $\bar{\upsilon}$ (Co—N) at 467 cm^{-1} [34].

From the theoretical calculations performed on the molecular structures of both the ligand and the cobalt complex, the vibration spectra obtained have been compared with the experimental ones (Figs. 2 and 3). The theoretical and experimental infrared spectra of the ligand show a good agreement to a large extent (Fig. 2). The vibration bands that appear between 2900 and 3500 cm^{-1} indicate a total agreement between the experimental and the calculations. However, the bands that exist on the experimental spectrum from 400 to 1700 cm^{-1} show a shift in the theoretical one toward the higher frequencies. The intense band that arises from the carbonyl vibration for instance, appears experimentally at 1639 cm^{-1} but theoretically at 1650 cm^{-1}. The one arising from the vibration of the (N—C═S) group also appears experimentally at 1575 cm^{-1} and at 1650 cm^{-1} on the calculated spectrum of the ligand.

The difference that appears between those two spectra can be attributed to a certain extent to the different physical states of the ligand. The experimental spectrum is obtained from a solid complex, in which exist interactions within the crystal system, but the calculated one results from an optimization in vacuum [35]. One can notice on the complex spectrum (Fig. 3) that the experimental broad band that arises from the vibration of the coordinated water molecules is well defined and resolved in the theoretical spectrum. Two different bands appear at 3560 and 3060 cm^{-1} that are attributed respectively to the vibration of the (O—H) and (N—H) bands.

The theoretical spectrum of the cobalt complex (Fig. 3) also shows the effect of the complexation on the ligand's bands. Starting from υ (C═O), all the bands involved in the delocalization that exists within the ligand's structure are shifted in different proportions to lower frequencies. A comparison between the two theoretical spectra of the ligand and its cobalt complex reveals two new bands at 520 cm^{-1} and 545 cm^{-1}. These bands are respectively attributed to the vibration of Co—N and Co—O, which is in good agreement with the experimental data that shows them at 467 and 501 cm^{-1} respectively [34].

3.3. Mass spectrometry

The spectrum of the cobalt complex shows a base peak at m/z = 515.5 (100%) corresponding to the formula $[Co(HL)_2]$ where the metal is coordinated to two deprotonated equivalent ligands. A good confirmation of the complex molecular weight was obtained from the molecular ion peak at (m/z^-) = 550 (20%) which corresponds to the

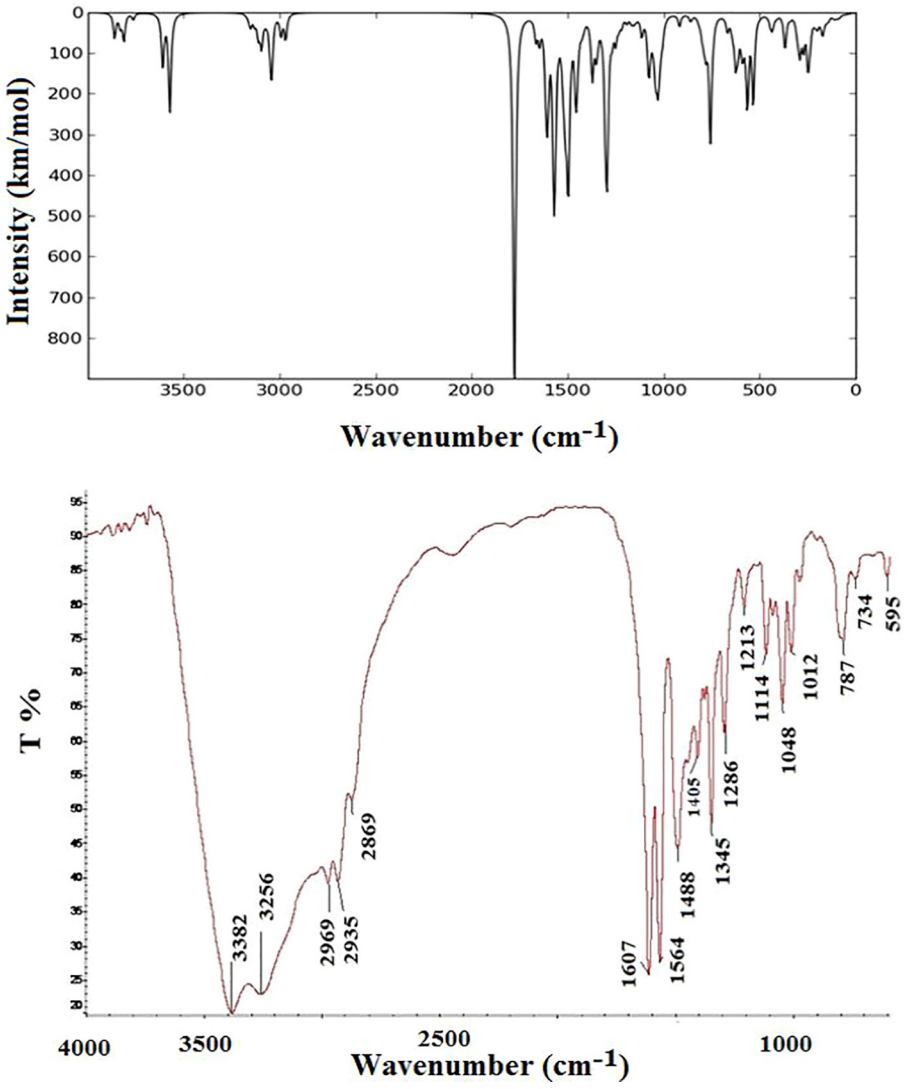

Fig. 3. Theoretical (upside) and experimental vibration spectra of the cobalt complex.

formula $[Co(HL)_2(H_2O)_2]$, which is in good agreement with the infrared results.

3.4. Magnetic properties

Magnetic susceptibility measurements were performed on powdered samples between 5 and 300 K. The temperature dependence of the effective magnetic moment, $\mu_{eff} = (8\chi_m T)^{1/2}$, and the reciprocal susceptibility are shown in Fig. 4. The μ_{eff} value at room temperature is 5.16 B.M. in good agreement with that expected for a magnetically isolated Co^{2+} in distorted octahedral arrangement, and allow us to assign an effective spin of S = 3/2 for the this compound at room temperature.

The magnetic moment slowly decreases from 300 to 50 K and more rapidly at lower temperatures, reaching a value of 3.7 BM at 5 K. The reciprocal molar magnetic susceptibility follows a Curie-Weiss law above 100 K (continuous line in Fig. 4), being the Curie constant $C_m = 3.83\ cm^3\ K/mol$ and $\theta = -46$ K. Both, the negative temperature intercept and the decrease observed in the effective magnetic moments when the temperature is lowered, must be ascribed to the effect of the first-order spin–orbit coupling typical of octahedral Co(II) compounds ($\lambda = -170\ cm^{-1}$ for the free ion [36]). Because of this and the crystalline distortions the lowest electronic state in octahedral field is a well-isolated spin doublet (S = 1/2), being the magnetic behaviour

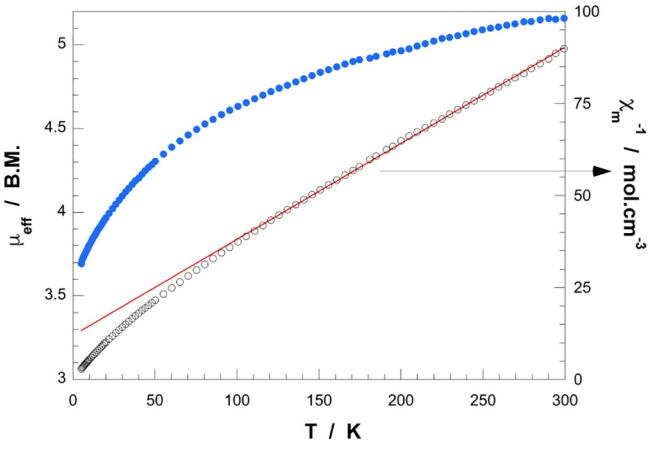

Fig. 4. Magnetic behaviour of the Co(II) complex.

qualitatively similar to that expected for a system with moderate antiferromagnetic interactions. The relatively high value of the magnetic effective moment at low temperature indicates a reduced orbital mixing between $^4T_{1g}(F)$ and $^4T_{1g}(P)$ terms, close to the weak-field limit [37].

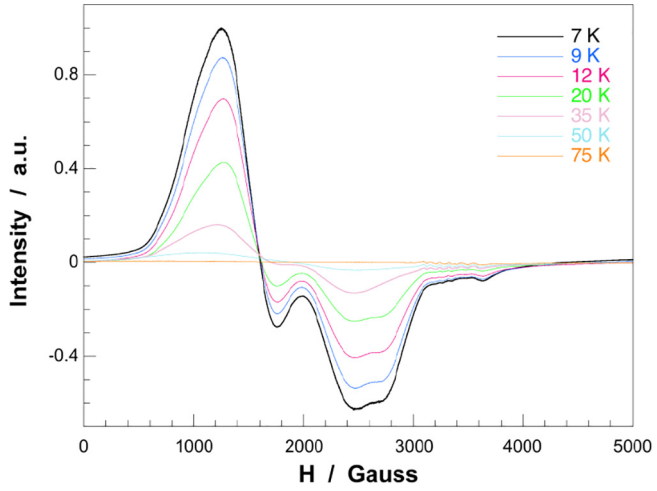

Fig. 5. X-band EPR spectra of the Co(II) complex at different temperatures.

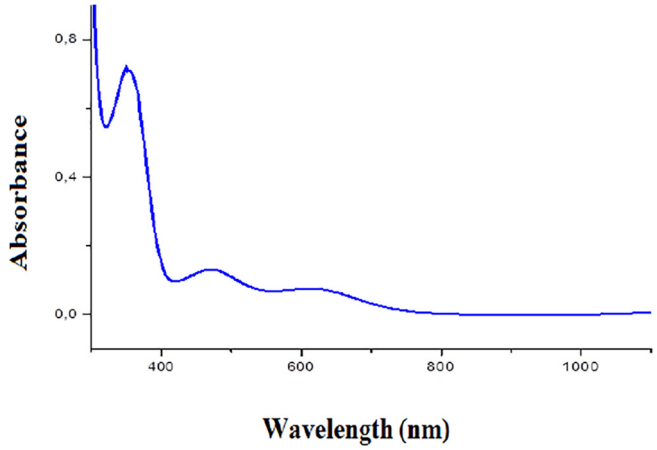

Fig. 6. Electronic spectrum of the cobalt complex.

3.5. EPR study

X band ESR spectra were recorded on powdered samples from 7 to 300 K (Fig. 5). The lowest temperature signal presents a poor resolution due to a rather large line width, but it shows the strong anisotropy of the g tensor usually observed for Co^{2+} ions in distorted octahedral environments [38]. The spectrum can be described in terms of a spin doublet $S_{eff} = 1/2$ arising from the splitting of the $^4T_1$ term through spin-orbit coupling and local distortion of the octahedral sites. The approximate g values are 6.3, 4.2 and 2.57, their sum being in good agreement with the theoretical value near 13 proposed by Abragam and Pryce [39]. Increasing the temperature up to 100 K caused a further broadening of the signal and above this temperature the compound became silent to ESR. This behaviour can be attributed to the very short spin-lattice relaxation time of the Co(II) ions in octahedral fields. The presence of excited states only a few hundred reciprocal centimetres above the ground state allows fast electronic relaxation near room temperature.

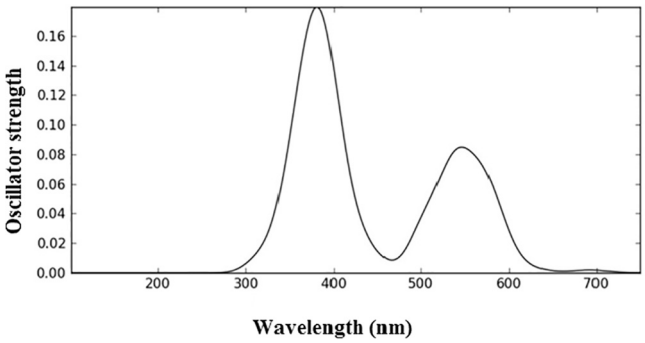

Fig. 7. Theoretical electronic spectrum of the cobalt complex.

3.6. Electronic spectral study

The electronic spectrum of the octahedral cobalt(II) complex with the pyrazolone ligand shows four bands (Fig. 6). Three bands arising from d-d transitions in an octahedral crystal field appear at 1064, 612 and 468 nm and correspond respectively to $^4T_{1g} \rightarrow {}^4T_{2g}$, $^4T_{1g} \rightarrow {}^4A_{2g}$ and $^4T_{1g}$ (^4F) $\rightarrow {}^4T_{1g}$ (^4P) transitions according to Tanabe-Sugano diagram [40]. The fourth and intense band that appears in the UV range at 354 nm is attributed to a charge-transfer band (Fig. 6). Table 2 summarizes the electronic data.

The structure of the cobalt complex has been optimized in ethanol in order to obtain its electronic spectrum that could be compared to the experimental one in the same solvent. Fig. 7 reports the theoretical spectrum of the complex between 300 and 800 nm considering 30 excited states.

The examination of the theoretical spectrum of the complex (Fig. 7) shows three bands between 300 and 800 nm. These bands are in intensity and position in agreement with the experimental ones (Table 3) although a slight red-shift is observed in the positions of the calculated bands. The intense band that appears in both spectra between 300 and 400 nm corresponds to a charge-transfer band. The nature of the band has been confirmed by the calculated oscillator strength (*f*) (Table 3). This parameter is an important one, as it helps approaching the nature of the bands, and allows a good comparison between the experimental and theoretical spectra [41]. The oscillator strength value obtained for the calculated charge-transfer band is 0.180 and 0.176 for the experimental one (3) (Table 3). The values are closed and confirm with *f* higher than 0.1, that these bands have a charge-transfer nature, and do not arise from d-d transitions which are symmetry forbidden (Table 3).

$$f = 4.6 \cdot 10^{-9} \cdot \varepsilon \cdot \Delta\bar{\upsilon}. \quad (3)$$

where:

f is the oscillator strength
ε The molar absorption coefficient
$\Delta\bar{\upsilon}$ The band width at half the high.

Table 2
Electronic data of the cobalt(II) complex.

	Wavelength (nm)	Wavenumber (cm^{-1})	Molar absorption coefficient ($L.mole^{-1}.cm^{-1}$)	Assignation
$[Co(HL)_2(H_2O)_2]$	1064	9400	35	$^4T_{1g} \rightarrow {}^4T_{2g}$
	612	16300	720	$^4T_{1g} \rightarrow {}^4A_{2g}$
	468	21400	1200	$^4T_{1g}$ (^4F) $\rightarrow {}^4T_{1g}$ (^4P)
	354	28200	7500	Metal-ligand charge transfer

Table 3
Experimental and calculated oscillator strengths in the range of 300–800 nm.

Experimental wavelengths (nm)	Calculated wavelengths (nm)	Experimental *f*	Calculated *f*
612	680	0.0094	0.0040
468	550	0.0230	0.0850
354	390	0.1760	0.1800

Theoretical calculations performed using TDDFT also allowed the determination of the Molecular Orbital contributions to the electronic transitions, which are interesting in the case of charge-transfer bands for which there are two possibilities: metal-ligand or ligand-metal charge-transfer transitions.

The data obtained from the TDDFT study shows that the band that appears between 350 and 400 nm arises from two main transitions. The first is a transition from alpha-HOMO to alpha-LUMO with a contribution of 37%. The second is a transition from Beta-HOMO to beta-LUMO + 3 with a contribution of 46%. The study of the orbitals distribution in the cobalt complex suggests that the transition here described arises from a metal-ligand charge-transfer, which is expected in the case of Co^{2+}, knowing its trend to oxidation, also confirmed by cyclovoltametry.

3.7. Cyclic voltammetry study

Cyclovoltammetry is an interesting way to explore the redox properties of a chemical compound, especially when this latter contains a metallic specie that can exist in several oxidation states [21,42]. The study starts with the measurement of the ligand cyclovoltammogram and a comparison with the one recorded for the complex. It helps giving the proper attribution of the peaks arising from the ligand or the metal. The voltammogram of the ligand previously studied [19] shows three anodic peaks and three cathodic ones. A rigorous examination of the complex cyclic voltammogram shows an additional irreversible anodic peak that appears at 0.5 V against ferrocene, attributed to the oxidation of Co(II) to Co(III). No cathodic peak involving Co(II) is observed (Fig. 8).

3.8. Molecular modeling of the pyrazolone and its metal complex

3.8.1. Optimization of the ligand H_2L structure

Quantum calculations have been performed on the pyrazolone ligand (H_2L) and the results obtained compared with the X-Ray data previously reported [19]. Fig. 9 reports the optimized structure of the ligand with selected bond lengths. The theoretical study of the two tautomeric forms of the ligand, which can exist in a thiol or thione

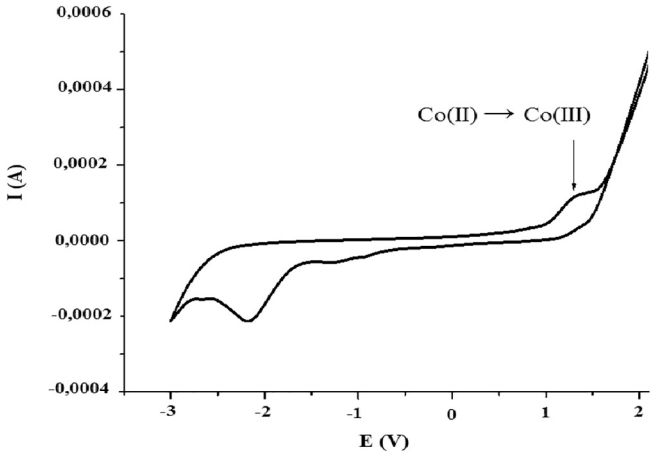

Fig. 8. Cyclovoltammogram of the cobalt(II) complex.

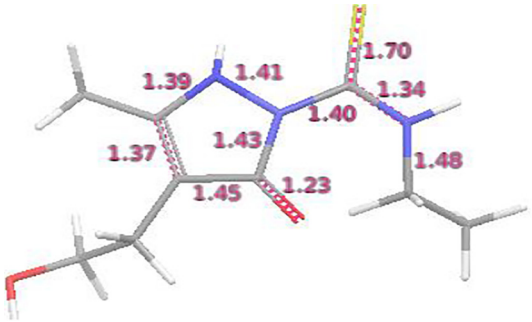

Fig. 9. Optimized structure of the ligand H_2L showing selected bond lengths.

form, shows that the thione form is the most stable in both gaseous state and in solution. This is consistent with the results of the NMR and the X-ray diffraction studies of the ligand [19].

The analyze of the bond lengths given in Fig. 9 shows that there is a delocalization within the molecule of the ligand, which is in agreement with the results of the X-rays which indicate that many bond lengths are between the simple bonds and the double ones. For instance, the double bonds of the unsaturated groups C═O, C═C and C═S respectively of 1.23; 1.37 and 1.70 Å are all longer than the corresponding conventional double bonds, respectively of 1.21; 1.34 and 1.53 Å. However, they are shorter than the corresponding single bonds. Single bonds involved in the conjugation such that the C−C and C−N heterocyclic bonds are shorter than the conventional single bonds of 1.53 and 1.47 Å.

3.8.2. Structure modeling of $[Co(HL)_2(H_2O)_2]$ and spectral features

The results of the complex characterization suggest the formula $[Co(HL)_2(H_2O)_2]$, where Co(II) is coordinated to two equivalent deprotonated molecules of the pyrazolone. The metal is also coordinated to two water molecules in a *cis* position resulting in an octahedral geometry (Fig. 10). Nevertheless, remain three possible structures. The axial positions can contain two nitrogen atoms, two sulfur atoms or a nitrogen and a sulfur. The calculations performed on all the possible structures indicated that the last, with the lowest energy, was the most stable structure. Figs. 11 and 12 report the optimized structure of the complex with respectively the bond lengths and the angles of the coordination sphere.

A careful examination of the lengths Co−N, Co−O and Co−S shows that they are closed to the corresponding bonds that we previously

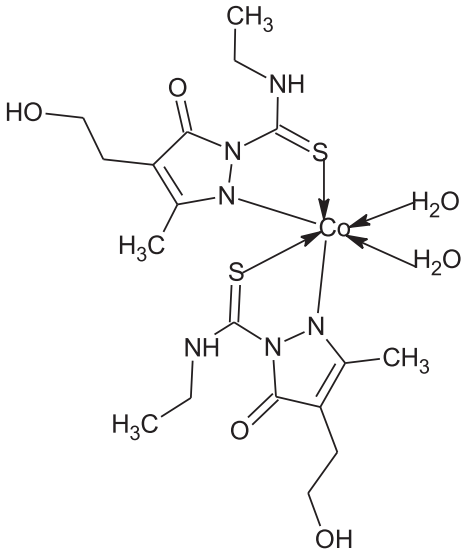

Fig. 10. Schema of $[Co(HL)_2(H_2O)_2]$ structure.

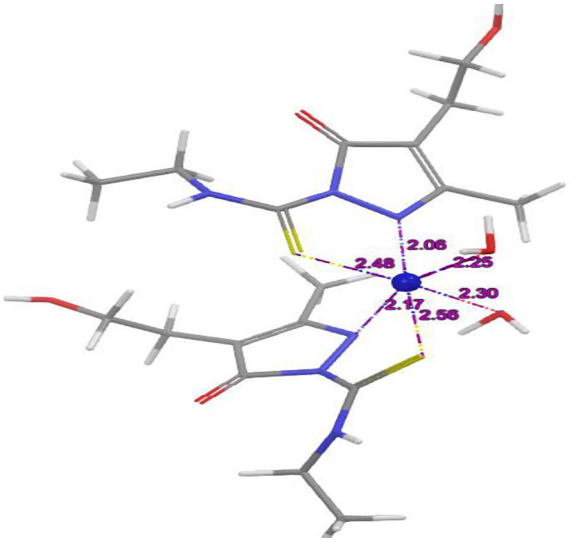

Fig. 11. Optimized structure of $[Co(HL)_2(H_2O)_2]$ indicating the bond lengths.

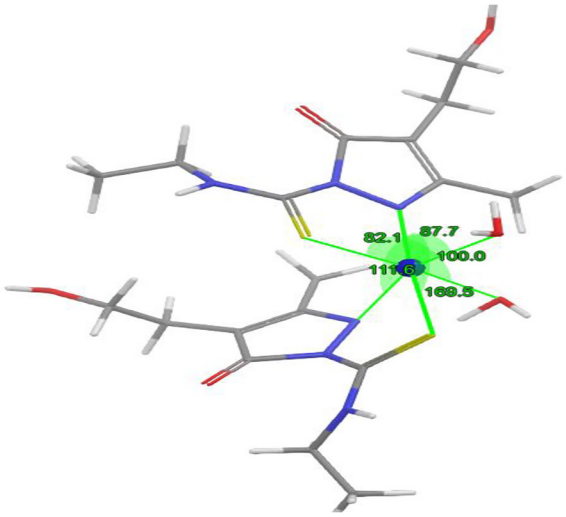

Fig. 12. Optimized structure of $[Co(HL)_2(H_2O)_2]$ indicating the angles in the coordination sphere.

reported from X-Ray structures for Cu(II) and Ni(II) with the same ligand [19]. The study of the angles reported in Fig. 12 shows that the structure is not a regular octahedral geometry. The angle N—Co—S formed by the atoms occupying the axial position, is equal to 169.5° which is 10.5° far from the 180° expected in a regular structure. The four angles formed by the atoms of the plane with the nitrogen of the axial position N—Co—S, N—Co—N, N—Co—O_1 and N—Co—O_2 are respectively of 82.1°; 111.6°; 100°; and 87.7° which make them differ with an average of 8° from a regular structure. O_1 and O_2 belong to the two water molecules of the complex.

Table 4
Frontier orbitals energies of the ligand and the cobalt complex (Energies given in Hartree).

Compound	E_{HOMO}		E_{LUMO}		GAP
Ligand in gas	−0.21963		−0.04843		0.17120
Ligand in ethanol	−0.22815		−0.05805		0.17010
Complex in gas	$E_{\alpha\text{-HOMO}}$	$E_{\beta\text{-HOMO}}$	$E_{\alpha\text{-LUMO}}$	$E_{\beta\text{-LUMO}}$	0.11141
	−0.18655	−0.18467	−0.07326	−0.04431	
Complex in ethanol	$E_{\alpha\text{-HOMO}}$	$E_{\beta\text{-HOMO}}$	$E_{\alpha\text{-LUMO}}$	$E_{\beta\text{-LUMO}}$	0.10664
	−0.19959	−0.19787	−0.09123	−0.05589	

Fig. 13 shows the complex structure with the charges carried by each atom. These charges are of *Natural Bond Orbitals* type (NBO). The Fig. 13 shows that the metal carries the charge +1.23. The oxygen atoms carry charges close to −1. Nitrogen and sulfur atoms carry respectively charges closed to −0.55 and −0.32 which is in agreement with their respective electronegativities. One can notice that the oxygen of the carbonyl carries the most negative charge of all the insaturated groups. This is due to the delocalization that exists within the ligand's structure in which the carbonyl exerts an attractive mesomere effect.

The electronic structures of the studied compounds can be investigated by the quantum chemical parameters like the energy of the highest occupied molecular orbital (E_{HOMO}), energy of the lowest unoccupied molecular orbital (E_{LUMO}), and *LUMO-HOMO* energy gap (ΔE). The finding data are grouped in the Table 4 and illustrated in Figs. 14 and 15. The HOMO and the LUMO that are called the frontier molecular orbitals are important parameters in the chemical reactivity. ΔE is an important stability index helping to characterize the chemical reactivity and kinetic stability of a compound [43].

Fig. 14 shows that the LUMO is more extended on the ligand that the HOMO. The thiocarbonyl sulfur is the atom that contributes most to the electron donor effect of the ligand. Contribute also the nitrogen atoms of the amine group and the oxygen of the carbonyl. The LUMO exists strongly around the thioamide group except the cyclic nitrogen. It is concentrated also around the atoms of the carbonyl group and the ethylenic substituted cyclic carbon.

In the cobalt complex, one can notice that the distribution of the LUMO does not change significantly. It decreases around the thioamide and the carbonyl groups (Fig. 15). It is interesting to note that unlike

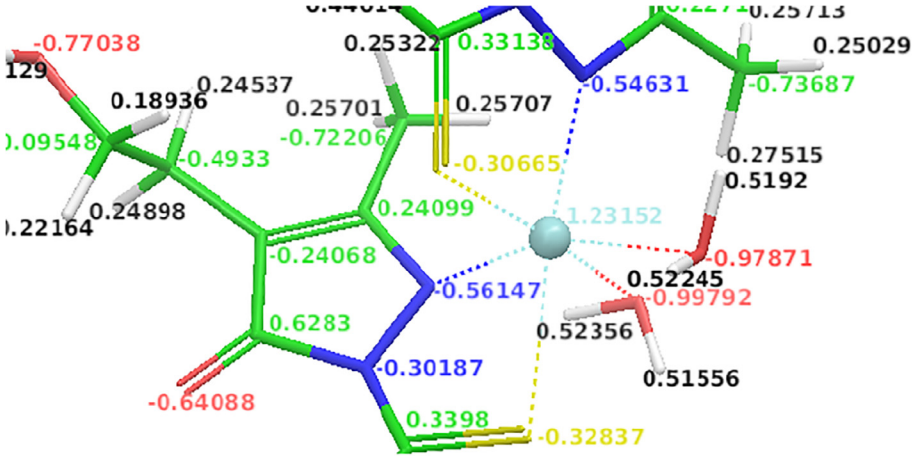

Fig. 13. Optimized structure of the cobalt complex showing the NBO charges.

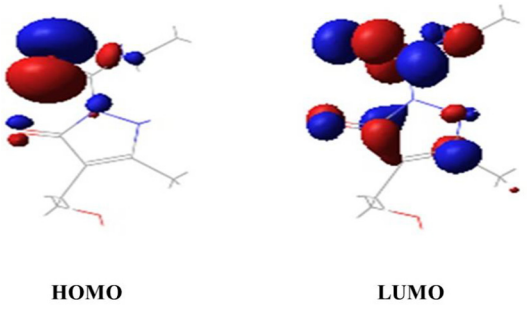

Fig. 14. Frontier molecular orbitals of the ligand in ethanol.

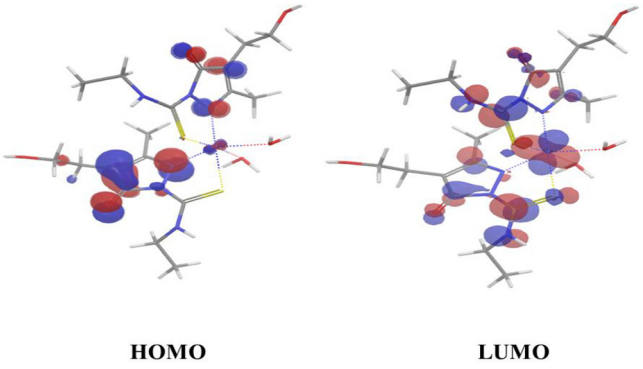

Fig. 15. Frontier Molecular orbitals plots of the cobalt complex in ethanol.

the LUMO, the distribution of the HOMO changes a lot from the ligand to the complex. The sulfur which contributes a lot to the HOMO of the ligand, does not contribute to the complex orbital anymore. The same thing is observed with the nitrogen atoms of the thioamide group. Fig. 15 shows that the central ion Co(II) brings an important contribution to the LUMO, which suggests electrophilic attack sites, but a weak one to the HOMO. Frontier orbitals energies of the pyrazolone and its cobalt complex are gathered in Table 4.

One can notice from Table 4 that all the energies of the frontier molecular orbitals, including those of spin-orbitals, are negative, which indicates the stability of the prepared compounds [44]. The cobalt complex has the smallest energy gap, in both gas and ethanol, which suggests a lowest kinetic stability than the free ligand; it easily offers electrons to an acceptor.

3.9. DNA binding affinity of the ligand H_2L and $[Co(HL)_2(H_2O)_2]$

3.9.1. DNA binding studies by electronic spectrometry

The electronic spectrometry can be an efficient tool for studying the potential interaction between a compound and DNA. The observation of the changes that appeared upon the titrations on both the ligand electronic spectrum and the complex one, clearly indicated that an interaction with DNA occured. An hypochromism appeared on the spectra of the ligand and the cobalt(II) complex upon the addition of increasing amounts of DNA (Figs. 16 and 17).

The hypochromism suggests that the interaction that exists is intercalative [45]. This phenomenon that takes place between planar molecules and DNA is due to a strong stacking interaction between the aromatic chromophore of the ligand and the DNA base pairs [46]. In this process, the compound inserts between two stacked base pairs of DNA and positions itself within the center of the DNA double helix. The intercalated molecule is stabilized by hydrophobic stacking interactions with adjacent base pairs [46]. The magnitude of the binding strength of the complexes with DNA can be evaluated by the value of the binding constant K_b.

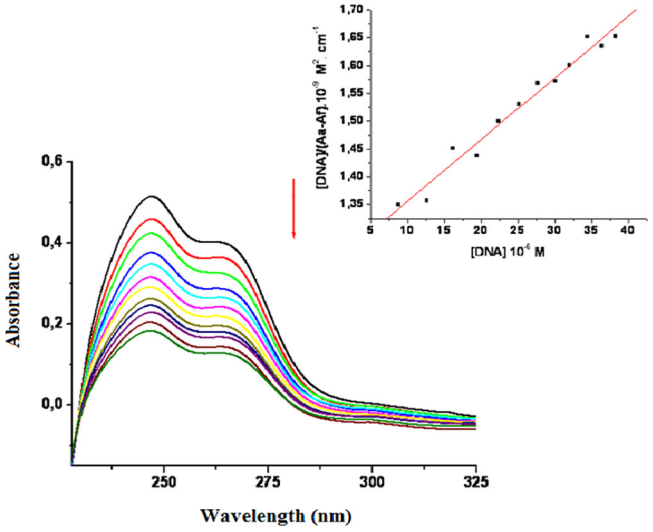

Fig. 16. Electronic spectrum of the ligand H_2L (20 μM) in buffer (containing 1% DMSO) with increasing amounts of DNA (0–40 μM). (Arrows show the changes upon the titration). In plot: $[DNA]/(\varepsilon_a - \varepsilon_f)$ vs. [DNA].

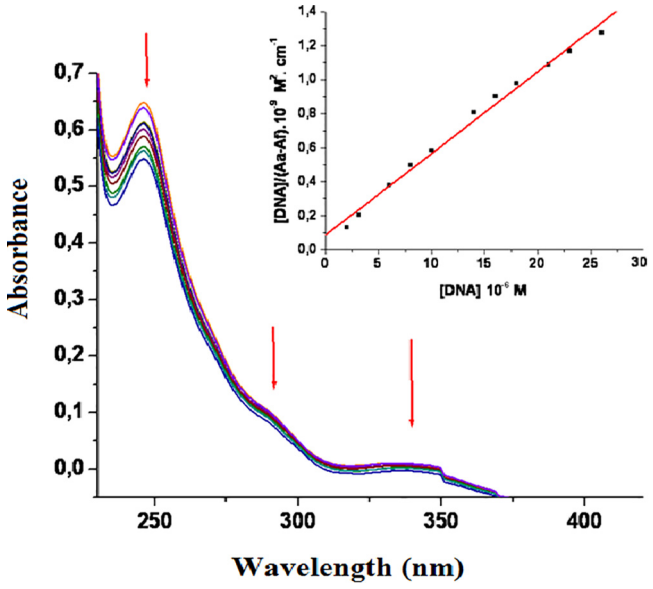

Fig. 17. Electronic spectrum of $[Co(HL)_2(H_2O)_2]$ (20 μM) in buffer (containing 1% DMSO) with increasing amounts of DNA (0–30 μM).

This latter is calculated by the Eq. (4) [47]

$$[ADN]/(\varepsilon_a - \varepsilon_f) = [ADN]/(\varepsilon_b - \varepsilon_f) + 1/Kb(\varepsilon_b - \varepsilon_f) \quad (4)$$

where ε_a is the apparent absorption coefficient corresponding to A_{obs}/[compound], ε_f the absorption coefficient of the free compound, and ε_b the absorption coefficient of the compound when fully bound to DNA. K_b is obtained by the ratio of slope to Y intercept in plots of $[DNA]/(\varepsilon_a - \varepsilon_f)$ *versus* [DNA] given in Figs. 16 and 17.

The binding values calculated for the ligand and its cobalt complex are respectively ($0.89 \times 10^4\ M^{-1}$) and ($1.99 \times 10^4\ M^{-1}$). These values suggest a moderate binding affinity to DNA, the cobalt binding affinity being comparable to many cobalt(II) complexes with (N,O) coordination environment [20,48]. The complexes of copper(II) and nickel(II) with the same ligand that we previously prepared and studied showed a weaker affinity to DNA in comparison with the cobalt complex [19]. In this series the best intercalator is the cobalt complex, followed by the nickel complex $[Ni(HL)_2(H_2O)]$ and the ligand. The weaker intercalator

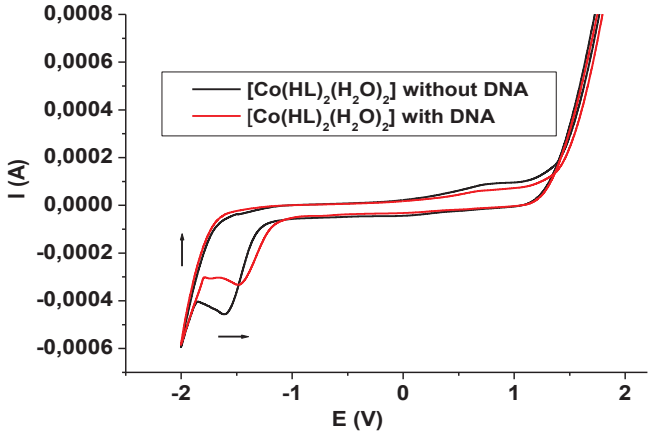

Fig. 18. Cyclovoltammogram of $[Co(HL)_2(H_2O)_2]$ in absence and presence of DNA. Arrows show the changes after the addition of DNA.

being the copper complex $[Cu(HL)_2(H_2O)]$.

The cobalt complex $[Co(HL)_2(H_2O)_2]$ shows a stronger binding strength that the free ligand. This may be attributed to the presence of another plane ligand in the structure of the complex (planeity previously showed by X-Rays [19] and DFT). In many cases of intercalation, the bigger is the planeity, the better is the binding strength [49]. It is important to note that this result is in perfect agreement with the theoretical DFT study which revealed the relative low stability of the complex in comparison with its ligand.

3.9.2. *DNA binding affinity studied by cyclic voltammetry*

Cyclic voltammetry is one of the most useful ways to reveal an interaction of an electroactive compound with DNA [21,42,49]. The cyclovoltammogram of the cobalt complex has been recorded first without DNA, and then with a solution (20 μM) of DNA in buffer (15 mM of trisodium citrate and 150 mM of NaCl at pH 7.2). The scan was performed from −2V to +2 V. No additional peaks were observed upon the addition of DNA. However, a clear decrease in the peaks intensities was observed, in addition to a shift of the potentials toward more positive values (Fig. 18). The decrease in the current intensity takes its origin from the existence of an equilibrium mixture of free and DNA-bound complex on the electrode surface [21,48].

The literature reports that the electrochemical potential of a small molecule shifts positively when it intercalates into the DNA double helix, and negatively when the molecule interacts with DNA electrostatically [48]. However, a positive shift of one peak and a negative one to another peak may suggest that the molecule can bind to DNA by both intercalation and electrostatic interaction [21]. The changes observed on the complex voltammogram confirm that an interaction exists between the cobalt complex and DNA, and indicates like the electronic spectrometry before, the intercalation as a binding mode.

3.10. *Cytotoxic properties of the ligand H_2L and the cobalt complex*

Most of the anticancer chemotherapeutic drugs that are broadly and successfully used today are DNA-damaging agents. Targeting DNA has proven to cause relatively potent and selective destruction of tumor cells [50]. Since both the ligand and the cobalt complex revealed an interaction with DNA through intercalation with relatively good binding abilities, especially in the case of the cobalt complex, they have been tested on two tumoral cell lines: PC-3 (human prostate carcinoma) and HT-29 (human colon carcinoma).

The method used for the study was the sulphorhodamine B (SRB) assay, which allows the evaluation of both the cytotoxic and cytostatic properties of a compound. Cisplatin and Transplatin were included as control drugs. The molecules under study did not show either cytostatic or cytotoxic activities over the concentration range used in the experiment (Table 5).

Table 5
Cytotoxic and cytostatic data of the ligand and the cobalt complex tested on prostate and colon cancer cells.

μM	PC3			HT29		
Compound	GI_{50}[a]	TGI[b]	LC_{50}[c]	GI_{50}[a]	TGI[b]	LC_{50}[c]
Ligand H_2L	> 100	> 100	> 100	> 100	> 100	> 100
$[Co(HL)_2(H_2O)_2]$	75	> 100	> 100	73	> 100	> 100
Cisplatin	0.7	20.9	> 30	3.8	8.7	19.2
Transplatin	0.2	> 30	> 30	> 30	> 30	> 30

[a] GI_{50}: 50% inhibition of the cellular division.
[b] TGI: Total inhibition of the cellular division.
[c] LC_{50}: 50% cells death.

A review of the literature reveals that many good DNA-binding compounds inhibit some cells proliferation and are not active at all on some others. A good example is the Cisplatin used here as a control drug, and which is the main platinum antitumor drug applied in clinical settings. This latter interacts well with DNA but is not effective on some cancer cells such as the ovarian [51,52]. Multidrug resistance is a major factor in the failure of many forms of chemotherapy. Resistance to treatment with anticancer drugs results from a variety of factors. The most common reasons for acquisition of resistance to a broad range of anticancer drugs is expression of one or more energy-dependent transporters that detect and eject anticancer drugs from cells, insensitivity to drug-induced apoptosis and induction of drug-detoxifying mechanisms. Studies on mechanisms of cancer drug resistance have yielded important informations about how to circumvent this resistance to improve cancer chemotherapy [53].

4. Conclusion

Our work described the synthesis and the characterization of an octahedral high spin Co(II) complex which contains a 5-pyrazolone that acts as a (N,S) bidentate monodeprotonated ligand. The complex which contains two water molecules in a *cis* position, has been studied in solution where two predominant complex species exist at different pH media: $[Co(HL)]^+$ and $[Co(HL)_2]$. After the characterization of the solid complex by several spectrometric and voltammetric methods, besides a rigorous DFT study of the structures and their features, the binding strength of our compounds with DNA has been explored and assessed by electronic spectrometry and cyclic voltammetry. The study revealed that intercalation takes place between both the pyrazolone, its complex and DNA, with relatively good binding abilities. Potential cytotoxic and/or cytostatic properties of the ligand and the cobalt complex have been explored but no cytotoxicity appeared over the concentration range. The combination of the binding abilities with the weak cytotoxic properties encouraged us to look deeper into our compounds profile, and to try other biological evaluations, with a larger series of metals.

Acknowledgement

We would like to thank the partial support of this research by the former Ministerio de Economía y Competitividad from Spain (Grant nos. CTQ2015-66164-R and CTQ2017-90802-REDT). We would also like to thank the valuable help and comments from P. Taylor (IVIC, Venezuela) and I. del Hierro (Universidad Rey Juan Carlos, Spain).

References

[1] D. Rogolino, A. Cavazzoni, A. Gatti, M. Tegoni, G. Pelosi, V. Verdolino, C. Fumarola, D. Cretella, P.G. Petronini, M. Carcelli, Eur. J. Med. Chem. 128 (2017) 140–153.
[2] M. Jopp, J. Becker, S. Becker, A. Miska, V. Gandin, C. Marzano, S. Schindler, Eur. J. Med. Chem. 132 (2017) 274–281.
[3] W. Wani, S. Prashar, S. Shreaz, S. Gómez-Ruiz, Coord. Chem. Rev. 312 (2016)

67–98.
[4] J. Chen, F. Peng, Y. Zhang, B. Li, J. She, X. Jie, Z. Zou, M. Chen, L. Chen, Eur. J. Med. Chem. 140 (2017) 104–117.
[5] R.C. Chisté, D. Ribeiro, M. Freitas, A. Leite, T. Moniz, M. Rangel, E. Fernandes, J. Inorg. Biochem. 155 (2016) 9–16.
[6] J.S. Möhler, T. Kolmar, K. Synnatschke, M. Hergert, L.A. Wilson, S. Ramu, A.G. Elliott, M.A.T. Blaskovich, H.E. Sidjabat, D.L. Paterson, G. Schenk, M.A. Cooper, Z.M. Ziora, J. Inorg. Biochem. 167 (2017) 134–141.
[7] M. Carcelli, D. Rogolino, M. Sechi, G. Rispoli, E. Fisicaro, C. Compari, N. Grandi, A. Corona, E. Tramontano, C. Pannecouque, L. Naesens, Eur. J. Med. Chem. 83 (2014) 594–600.
[8] M.A. Santos, K. Chand, S. Chaves, Coord. Chem. Rev. 327–328 (2016) 287–303.
[9] G.P. Talwar, L.M. Srivasatava, Textbook of Biochemistry and Human Biology, PHI Learning, New Delhi, 2002.
[10] M.A. Cser, Metal Ions in Biology and Medicine vol. 8, John Libbey, Paris, 2004.
[11] F. Dimiza, A.N. Papadopoulos, V. Tangoulis, V. Psycharis, C.P. Raptopoulou, D.P. Kessissoglou, G. Psomas, J. Inorg. Biochem. 107 (2012) 54–64.
[12] E. Kouris, S. Kalogiannis, F. Perdih, I. Turel, G. Psomas, J. Inorg. Biochem. 163 (2016) 18–27.
[13] S.R. Morcelli, É.S. Bull, W.S. Terra, R.O. Moreira, F.V. Borges, M.M. Kanashiro, A.J. Bortoluzzi, L.L.F. Maciel, J. Carlos de A. Almeida, J. Inorg. Biochem. 161 (2016) 73–82.
[14] J.L. Li, L. Jiang, B.W. Wang, J.L. Tian, W. Gu, X. Liu, S.P. Yan, J. Inorg. Biochem. 145 (2015) 19–29.
[15] K.M. Vyas, R.V. Devkar, A. Prajapati, R.N. Jadeja, Chem.-Biol. Interactions 240 (2015) 250–266.
[16] P. Gunasekaran, S. Perumal, P. Yogeeswari, D. Sriram, Eur. J. Med. Chem. 46 (2011) 4530–4536.
[17] E.S. Badawey, I.M. El-Ashmawey, Eur. J. Med. Chem. 33 (1998) 349–361.
[18] T. Watanabe, S. Yuki, M. Egawa, H. Nishi, J. Pharmacol. Exp. Ther. 268 (1994) 1597–1604.
[19] S. Akcha, L. Hammal, S. Triki, L. Lezama, B. Nedjar-Kolli, O. Benali Baitich, J. Coord. Chem. 68 (2015) 4373–4394.
[20] C. Protogeraki, E.G. Andreadou, F. Perdih, I. Turel, A.A. Pantazaki, G. Psomas, Eur. J. Med. Chem. 86 (2014) 189–201.
[21] G. Psomas, J. Inorg. Biochem. 102 (2008) 1798–1811.
[22] S. Tsiliou, L.-A. Kefala, F. Perdih, I. Turel, D.P. Kessissoglou, G. Psomas, Eur. J. Med. Chem. 48 (2012) 132–142.
[23] M.L. Glówka, M. Baszczyk, C.H. Prentjas, D. Kovala-Demertzi, Pol. J. Chem. 78 (2004) 2013.
[24] L.J. Bellamy, The Infrared Spectra of Complex Molecules, second ed., Wiley, New York, 1964.
[25] V.I. Vetrogon, N.G. Lukyanenko, M.J. Schwing-Weill, F. Arnaud-Neu, Talanta 41 (1994) 2105–2112.
[26] Jaguar, version 8.2, Schrödinger, LLC, New York, NY, 2015.
[27] A.D. Bochevarov, E. Harder, T.F. Hughes, J.R. Greenwood, D.A. Braden, D.M. Philipp, D. Rinaldo, M.D. Halls, J. Zhang, R.A. Friesner, Int. J. Quant. Chem. 113 (2013) 2110–2142.
[28] A.R. Higuera-Padilla, J. Capote, D. Ortega, W. Castro, M. Rodriguez-Cordero, D. Coll, F. Hernández-Medina, M. Fernández-Mestre, I. Urdanibia, P. Taylor, B. Rodriguez, A. Karam, Polyhedron 102 (2015) 321–328.
[29] O. Sánchez, S. González, M. Fernández, A.R. Higuera-Padilla, Y. Leon, D. Coll, A. Vidal, P. Taylor, I. Urdanibia, M.C. Goite, W. Castro, Inorg. Chim. Acta 437 (2015) 143–215.
[30] S. Belaid, S. Djebbar, O. Benali Baitich, M.A. Khan, G. Bouet, C.R. Chim. 10 (2007) 568–572.
[31] N. Lechani, M. Hamdi, F. Aklil, S. Khabouche, O. Benali Baitich, D. Kheffache, S. Moussi, O. Ouamerali, Eur. J. Chem. 3 (2013) 285–291.
[32] J. Burgess, Ions in Solution, second ed., Woodhead Publishing, Cambridge, 1999.
[33] A.E. Martell, R.D. Hancock, Metal Complexes in Aqueous Solutions, Plenum Press, New York, 1996.
[34] S.A. Patil, C.T. Prabhakara, B.M. Halasangi, S.S. Toragalmath, P.S. Badami, Spectrochim. Acta Part A 137 (2015) 641–651.
[35] M.I. Orif, M.H. Abdel-Rhman, Polyhedron 98 (2015) 162–179.
[36] F.E. Mabbs, D.J. Machin, Magnetism and Transition Metal Complexes, Chapman and Hall, London, 1973.
[37] R.L. Carlin, Magnetochemistry, Springer, Berlin, 1986.
[38] R. March, W. Clegg, R.A. Coxall, L. Cucurull-Sánchez, L. Lezama, T. Rojo, P. González-Duarte, Inorg. Chim. Acta. 353 (2003) 129–138.
[39] A. Abragam, M.H.L. Pryce, Proc. R. Soc. (Lond.), Sect. A 206 (1951) 173.
[40] A.B.P. Lever, Inorganic Electronic Spectroscopy, Elsevier, Amsterdam, 1984.
[41] N. Tidjani-Rahmouni, N.H. Bensiradj, S. Djebbar, O. Benali-Baitich, J. Mol. Struct. 1075 (2014) 254–263.
[42] M. Nandy, D.L. Hughes, G.M. Rosair, R.K. Bhubon Singh, S. Mitra, J. Coord. Chem. 67 (2014) 3335–3353.
[43] O.A. El-Gammal, T.H. Rakha, H.M. Metwally, G.M. Abu El-Reach, Spectrochim. Acta A 127 (2014) 144–156.
[44] B. Dede, I. Ozmen, F. Karipcin, Polyhedron 28 (2009) 3967–3974.
[45] K.M. Vyas, R.N. Jadeja, D. Patel, R.V. Devkar, V.K. Gupta, Polyhedron 80 (2014) 20–33.
[46] R.R. Sinden, DNA Structure and Function, Academic Press, San Diego, CA, 1994.
[47] A. Wolfe, G.H. Shimer Jr, T. Meehan, Biochemistry 26 (1987) 6392–6396.
[48] F. Dimiza, A.N. Papadopoulos, V. Tangoulis, V. Psycharis, C.P. Raptopoulou, D.P. Kessissoglou, G. Psomas, Dalton Trans. 39 (2010) 4517–4528.
[49] R.R. Duan, L. Wang, W.Q. Huo, S. Chen, X.H. Zhou, J. Coord. Chem. 67 (2014) 2765–2782.
[50] K. Gurova, Future Oncol. 5 (2009) 1685–1713.
[51] D.W. Shen, L.M. Pouliot, M.D. Hall, M.M. Gottesman, Pharmacol Rev. 64 (2012) 706–727.
[52] P. Perego, S. Romanelli, N. Carenini, I. Magnani, R. Leone, A. Bonetti, A. Paolicchi, F. Zunino, Ann Oncol. 9 (1998) 423–453.
[53] M. Gottesman, Annu. Rev. Med. 53 (2002) 615–642.